JOURNAL OF MATERIALS SCIENCE 30 (1995) 4019–4026

Response of spray-deposited, stirred-cast and conventional cast Pb–Sn alloys to deformation in the semi-solid state

C.P. CHEN, C.-Y. A. TSAO
Department of Materials Science and Engineering, National Cheng Kung University, Tainan, Taiwan

Pb-35 wt% Sn alloys were deformed in the semi-solid state. The effects of the initial microstructures, deformation temperatures and deformation rates on the microstructures and the formability of the alloy were studied. A physical phenomenological model is proposed to explain the different behaviours of the stress–strain curves of semi-solid forming of various materials under various conditions. Three different processes, spray deposition (S/D), semi-solid synthesizing (SSS) and conventional casting (CC) were used to produce the Pb-35 wt% Sn alloys with different initial microstructures. Two strain rates, (0.083 and 0.00083 s^{-1}) and two deformation temperatures, (190 and 200 °C) were used in this study. There is no significant variation in particle size and in sphericity during semi-solid forming of Pb-35 wt% Sn alloys. The deformation stress increases monotonically as strain increases during semi-solid deformation of S/D materials, which consist of smaller solid particles. However, for SSS and CC materials, which consist of larger solid particles, the deformation stress increases in the beginning to a local maximum, then decreases to a minimum before it starts to increase again as strain increases. This phenomenon is more noticeable at lower deformation temperatures and higher strain rates. The deformation stresses required for deformation at higher deformation rates and at lower deformation temperatures are larger than those at lower deformation rates and at higher deformation temperatures, respectively.

1. Introduction

Semi-solid forming (SSF) is an effective net-shape forming process deforming metals in the semi-solid state, combining the elements of both casting and forging [1–3]. The study on the behaviours of metals in the semi-solid state was pioneered by Spencer and co-workers at MIT in 1971 [4]. He applied a shear strain on solidifying Sn-15% Pb alloy, and discovered a remarkable reduction in shear stress compared with those that were not sheared during solidification. The grain structure of the sheared alloy was non-dendritic, as opposed to the dendritic structure of not-sheared alloy. Since this early work, semi-solid processing (SSP), including semi-solid synthesizing (SSS) and semi-solid forming (SSF), has become a widely studied and accepted process. Compared with conventional cast (CC) materials, SSP materials have less segregation and finer grain size. Practically, SSP can increase part-forming rate, reduce the thermal shock imposed on the mould, increase mould life and reduce the force applied during forming [1–16].

Spray deposition (S/D) is an emerging advanced materials processing method [17–23]. In the process, a controlled stream of molten metal is atomized by pulsed high-velocity gas. The resulting spray of liquid metal droplets is directed towards a water-cooled substrate, where a preform is built up by continuous deposition of splatted liquid and semi-liquid droplets. The process is a hybrid rapid solidification process, because the metal experiences rapid cooling from the liquid state to the solid state, followed by rapid though somewhat slower solid state cooling to low temperature. This results in equiaxed, non-dendritic grains, fine microstructures, absence of macrosegregation, extended solid state solubility, and low oxygen content, in addition to minimum matrix/reinforcement chemical interaction and no reinforcement segregation for spray-deposited metal matrix composites. The density of the preforms, on average, falls in the range of $96 \pm 3\%$, which, together with the fine microstructures and absence of macrosegregation, eliminates the need for subsequent high temperature soaking and extensive deformation processing. Some spray-deposited alloys, because of fine equiaxed grained structures, exhibit unique thixotropic and/or superplastic behaviour [22].

The objective of this work was to study the deformation behaviours of Pb-35 wt% Sn alloys in the semi-solid state, which were produced by SSP, S/D and CC processes. The samples were heated to the

0022–2461

TABLE I The experimental parameters used for each sample

Sample	Material process	Deformation temperature	Initial strain rate
44	S/D	–	–
41	S/D	200	–
33	S/D	190	0.00083
32	S/D	190	0.08300
35	S/D	200	0.00083
37	S/D	200	0.08300
45	SSS	–	–
42	SSS	200	–
22	SSS	190	0.00083
23	SSS	190	0.08300
24	SSS	200	0.00083
25	SSS	200	0.08300
46	CC	–	–
43	CC	200	–
38	CC	190	0.00083
27	CC	190	0.08300
28	CC	200	0.00083
29	CC	200	0.08300

desired temperatures in the semi-solid region and deformed. In the experiment, the effects of the initial microstructures and the temperatures and strain rates of the deformation on the microstructures and the deformation behaviours of the samples were studied.

2. Experimental methods

Pb-35 wt % Sn samples were prepared by S/D, SSP and CC processes to obtain different initial microstructures. S/D samples were obtained with 5 kg cm^{-2} (70 p.s.i.) atomization pressure, 40 cm (15.7 inch) flight distance and 100 °C superheat; details of this process can be found elsewhere [17–20]. SSP samples were obtained by continuously cooling Pb-35 wt % Sn melt from 255 to 234 °C at an average cooling rate of 1.2 °C min^{-1} while the melt was stirred, before quenching at 234 °C. CC samples were obtained from the same process procedure as that of SSP samples, but no stirring was involved.

The dimensions of the samples used for SSF were 12 mm (0.47 inch) in diameter and 12 mm (0.47 inch) in length. Semi-solid forming (SSF) was performed with an Instron machine, model 1125. The samples were placed between two graphite plates, through the centre of which thermocouples were inserted to contact the samples directly from the top and the bottom. A three-zone temperature-controlled furnace was used to control the temperature distribution of the samples with the feedbacks from the thermocouples. The differences in temperatures between the top and bottom of the compacts were controlled to be within ± 2 °C. Nitrogen gas was fed through the heating zone.

Two semi-solid deformation temperatures, 190 and 200 °C, were chosen to study the effects of the deformation temperatures, both of which are in the liquid-plus-solid two-phase regime, which are from 250 to 183 °C. The samples were heated to the set temperature for semi-solid deformation, then held for 10 min to equalize the temperature within the samples before the onset of semi-solid deformation. Two deformation speeds, 0.6 mm min^{-1} (0.024 inch min^{-1}) and 60 mm min^{-1} (2.4 inch min^{-1}), corresponding to initial strain rates of 8.3×10^{-4} and 8.3×10^{-2} s^{-1}, respectively, were used to study the effects of the deformation rates. Table I lists the experimental parameters used for each sample. The samples were deformed from 12 mm (0.47 inch) high to 6 mm (0.24 inch) high, corresponding to a true strain of -0.69. The samples were quenched immediately after the deformation to preserve the as-deformed microstructures of the compacts. The force versus displacement relationships were recorded. In order to evaluate the microstructures of S/D, SSS and CC materials just before the deformation, the samples were also held at 200 °C for 10 min, and then quenched to room temperature without performing any deformation experiment.

An optical microscope, stereoscope and image analyser were used to study and analyse the microstructures, the distribution and the size of the primary phase.

3. Results and discussion

Fig. 1 shows the microstructures of the Pb–Sn alloys produced by S/D (spray deposition), SSS (semi-solid synthesizing) and CC (conventional casting). The as-S/D microstructure ("as" signifying not deformed in semi-solid state) is a non-dendritic structure with a very fine primary Pb phase as shown in Fig. 1(a), which is typical of the structures of S/D materials [17–20]. The average size of the primary Pb phase is about 25 μm. The average sphericity of the primary Pb phase is 0.59, which is obtained by using a two-dimensional sphericity analysis with the following formulation: sphericity $= 4\pi a/b^2$ where a = area of the particles and b = perimeter of the particles. The eutectic phase consists of Sn phase and spheroidized Pb phase due to slow solid-state cooling after deposition. The microstructure of as-SSS alloys shows as-quenched structure, consisting mainly of a rosette type of microstructure with eutectic phase in between, as shown in Fig. 1(b). This rosette type of structure was evolved from dendritic structures during semi-solid stirring, during which the dendritic structures were deformed and bent by shear force and by impact among themselves, together with particle spheroidizing and coarsening, resulting in individual rosette types of primary structure [1]. The average individual particle size within the rosette is 164 μm, and the average sphericity is 0.57. Fig. 1(c) shows the as-CC structure, which consists of conventional dendritic structures with an average SDAS (secondary dendrite arm spacing) of about 36 μm.

Fig. 2 shows the microstructures of the S/D, SSS and CC materials just before the onset of the semi-solid deformation. Fig. 2(a) shows the microstructure of the S/D material, which has similar particle morphology as that of as-S/D material. A slight increase in the primary particle size from original 25 to 35 μm is observed due to ripening during holding at 200 °C for 10 min with no significant increase in sphericity. The SSS material, however, shows a structure of bimodal

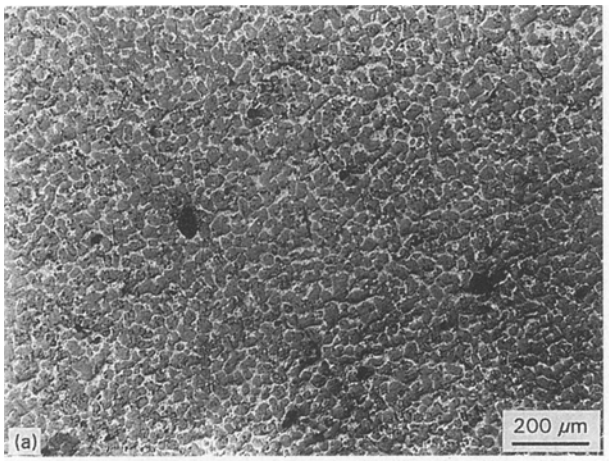

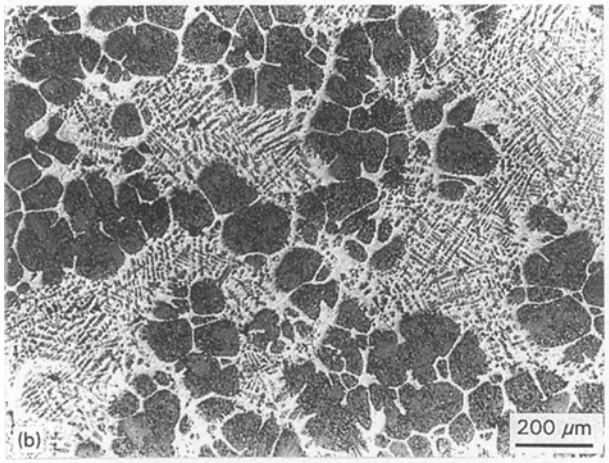

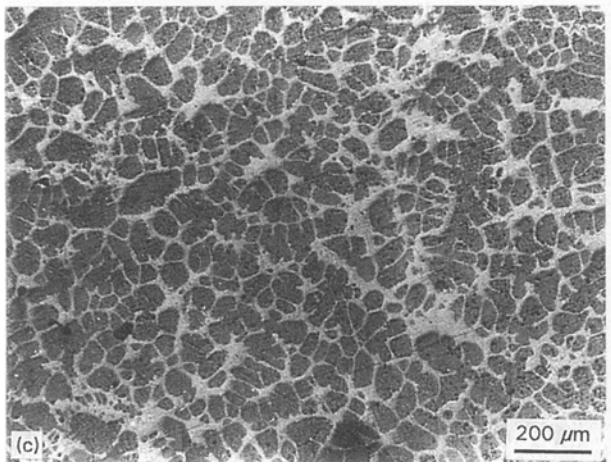

Figure 1 The microstructures of the Pb–Sn alloys. (a) As-S/D microstructure; (b) As-SSS microstructure; (c) As-CC microstructure.

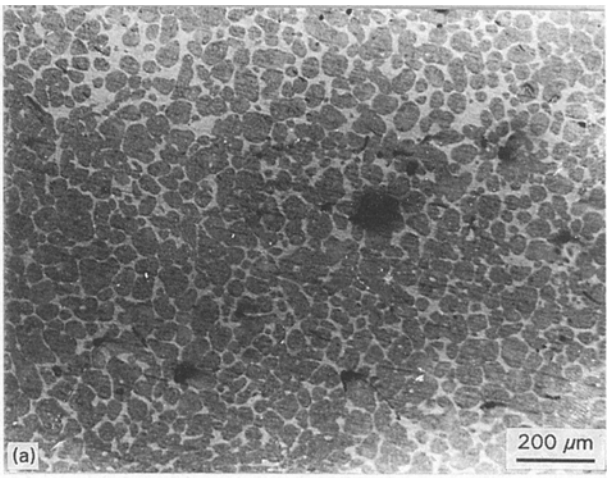

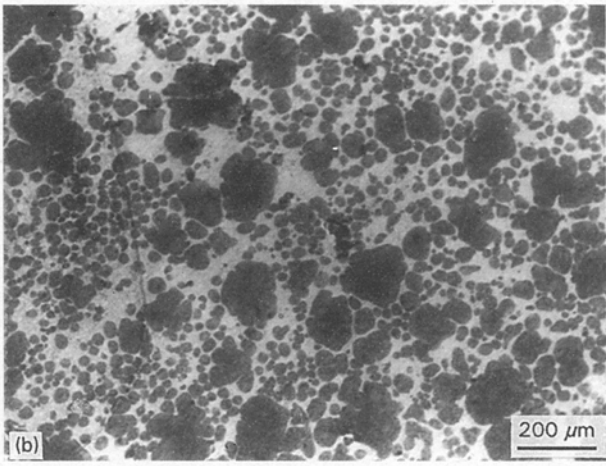

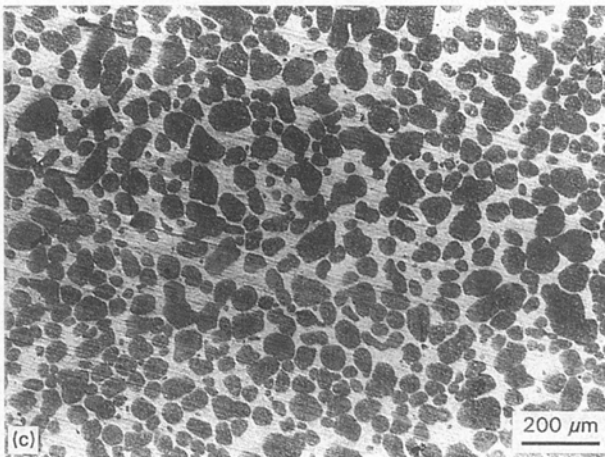

Figure 2 The microstructures of (a) S/D materials; (b) SSS materials; and (c) CC materials, held at 200 °C for 10 min, just before the onset of the semi-solid deformation.

primary particle distribution with two peak particle sizes, which are about 50 and 170 μm as shown in Fig. 2(b). The larger particles are the result of the breaking-up of the original rosette structure due to spheroidizing and Ostwald ripening during heating and holding at elevated temperature. The small particles were developed from spheroidizing and Ostwald ripening of the Pb phase in the original eutectic phase. Fig. 2(c) shows the structure of the CC material, which is very similar to that of the S/D material, showing spheroidized structure. However, the origin of the spheroidized structure of the CC materials is different from that of the S/D materials. The latter is the original as-spray-deposited structure, while the former is the result of both spheroidizing and ripening of the original as-cast dendritic structure. In addition, the average particle size of the CC material is about 99 μm, which is much larger than that of S/D material, which is about 35 μm.

The microstructures of the S/D, SSS and CC materials after the semi-solid deformation at various

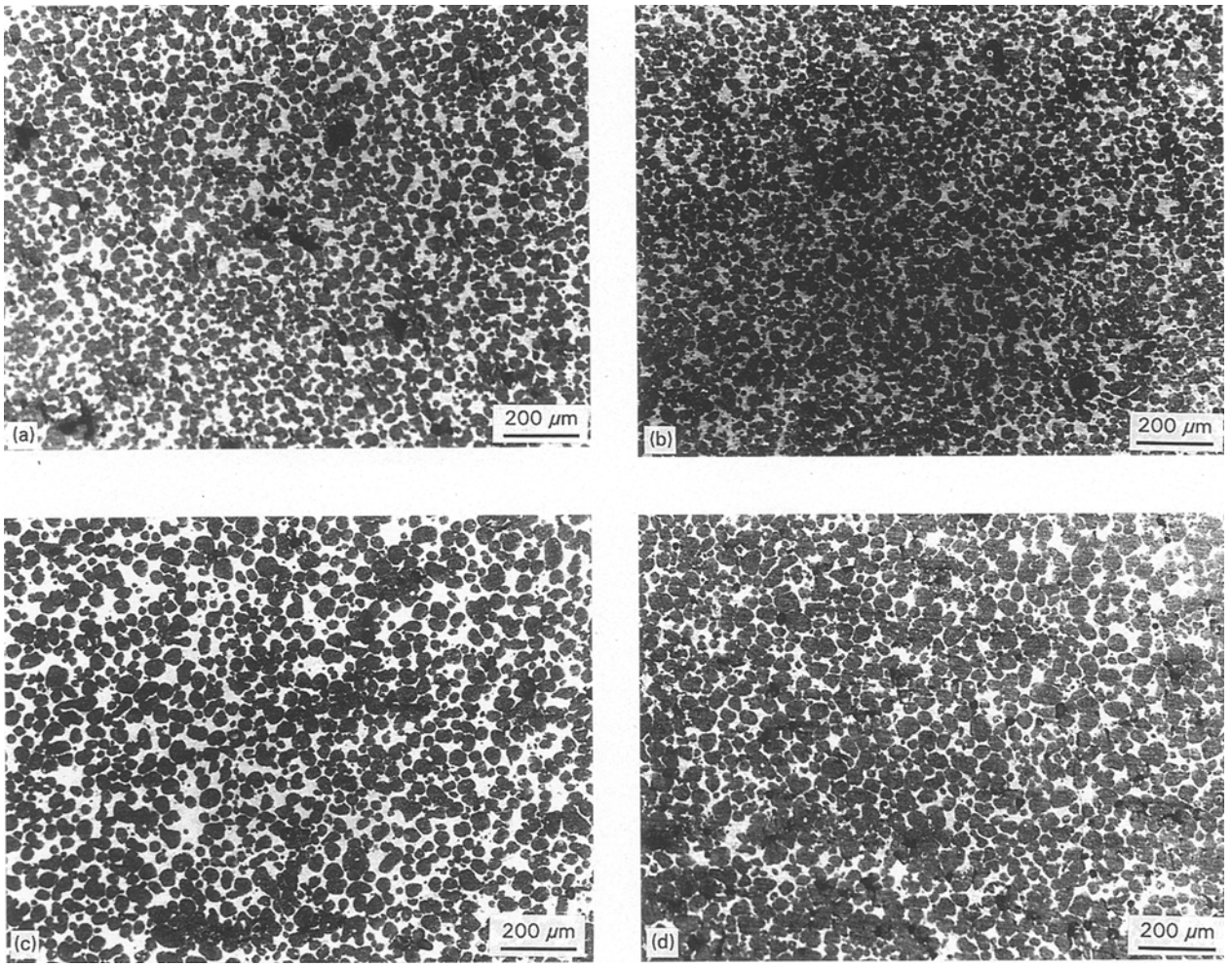

Figure 3 The microstructures of the S/D material after the semi-solid deformation at (a) 190 °C, 0.00083 s^{-1}; (b) 190 °C, and 0.083 s^{-1}; (c) 200 °C, and 0.00083 s^{-1}; and (d) 200 °C, and 0.083 s^{-1}.

deformation temperatures and deformation rates are shown in Figs 3–5, respectively. Fig. 3 shows the as-SSF microstructures of the S/D materials, which are similar to that of non-deformed S/D material shown in Fig. 2(a), consisting of fine non-dendritic structures. The average primary particle sizes and the sphericities of deformed structure are not significantly different from those of non-deformed structures. The as-SSF microstructures of the SSS materials are shown in Fig. 4, which are similar to those of non-deformed SSS material shown in Fig. 2(b), consisting of particles with bimodal distributions of particle size, which are not significantly different from that of non-deformed structure. Fig. 5 shows the as-SSF microstructures of the conventional-cast materials, which consist of spheroidized primary particles, and the average particle sizes are not significantly different from that of non-deformed CC material. The structures are similar to those of the S/D materials, except the primary particle sizes are much larger than those of the S/D materials.

Figs 6–9 show the effects of deformation strain rates on the stress versus strain relationships of the semi-solid deformation at various deformation temperatures. At 190 °C, the S/D materials show the lowest deformation stress, and behave differently from the SSP and CC materials, as shown in Figs 6 and 7. The stresses for both the SSP and CC materials show an increase at the beginning, reaching a maximum, then decreasing to a minimum before increasing again. However, the S/D materials behave differently, which show a continuous increase of stress as strain increases. The difference in these behaviours can be explained in terms of the sizes of the primary particles. The average primary particle sizes of both SSP and CC materials are in the order of 100 μm, which is much larger than those of the S/D materials, which are in the order of 30 μm. A physical phenomenological model described as follows is proposed here to explain the behaviours of the stress–strain curves of the semi-solid deformed Pb–Sn materials.

Four main physical mechanisms are operating during the semi-solid deformation, which are:

1. rearrangement of the solid particles;
2. flow of the liquid phase;
3. compression of the liquid phase; and
4. plastic deformation of the solid particles.

The force required to operate the flow of the liquid phase mechanism is the smallest, while the force required to operate the plastic deformation of the solid particles mechanism is the largest. The force required to operate the mechanism of compression of the liquid phase is larger than that to operate the mechanism of

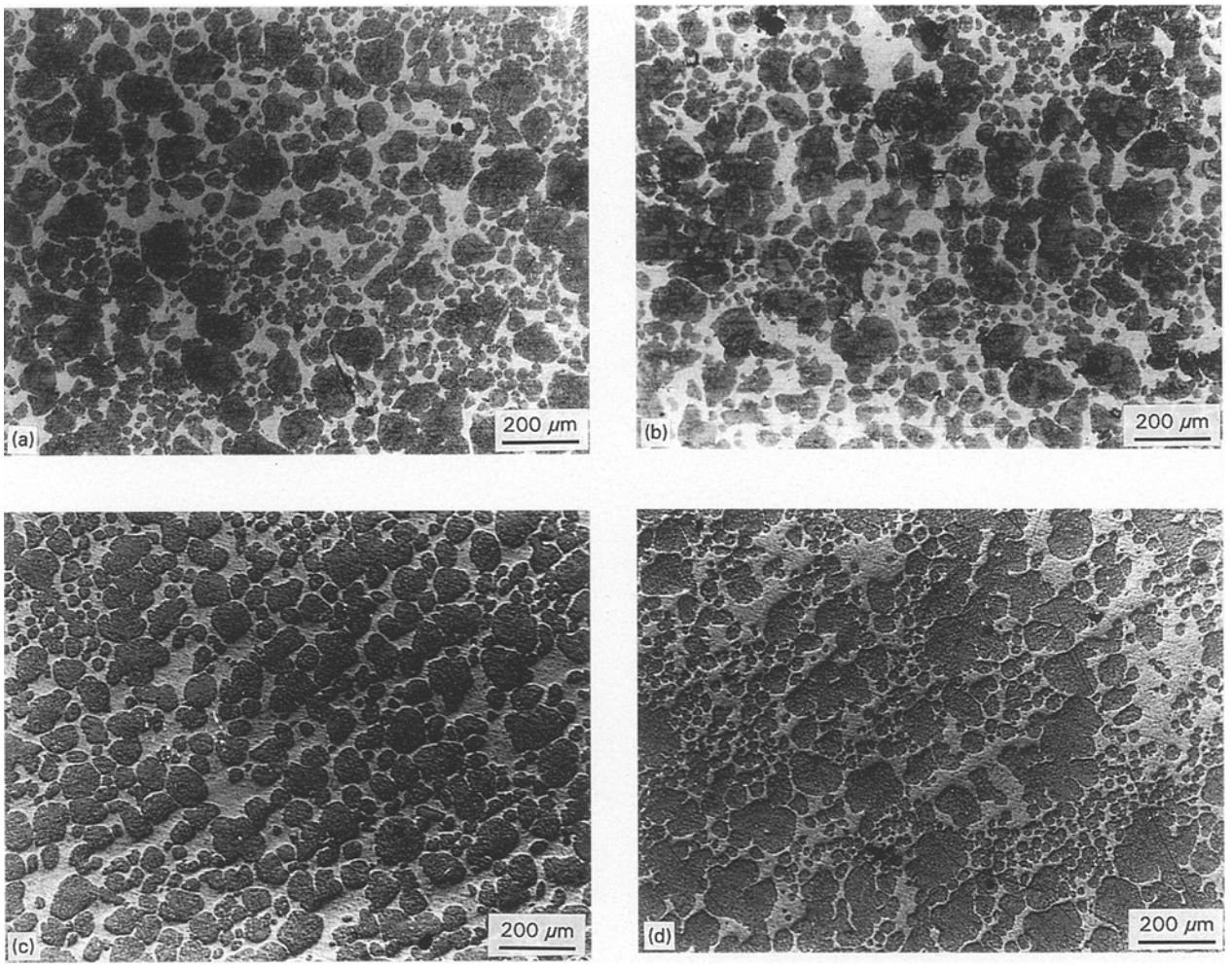

Figure 4 The microstructures of the SSS material after the semi-solid deformation at (a) 190 °C, and 0.00083 s^{-1}; (b) 190 °C, and 0.083 s^{-1}; (c) 200 °C, and 0.00083 s^{-1}; and (d) 200 °C, and 0.083 s^{-1}.

rearrangement of the solid particles. However, it is important to realize the following:

1. the flow of liquid mechanism can enhance the rearrangement of solid particles mechanism, and vice versa;
2. the mechanism of rearrangement of the solid particles is more time-dependent than other mechanisms, which means that the former is more sensitive to the variations of deformation rates;
3. larger solid particles are more difficult to be rearranged than smaller particles.

At onset of the deformation, the deformation stress increases as strain increases to deform the materials. In the initial stage of the semi-solid deformation, all four mechanisms can operate simultaneously; however, the mechanisms of rearrangement of solid particles and flow of liquid dominate, since both of them require less force than the other two mechanisms to operate. At the very beginning of the deformation, flow of liquid is the only significant mechanism, since it does not require time to be operative while rearrangement of solid particles mechanism does. As a result, the liquid phase is pushed towards the edge of the deformation compact, resulting in a larger solid fraction at the centre of the compacts than at the edges, as indicated by comparing the solid fraction at the centre with that at the edges [9]. Once the mechanism of flow of liquid operates, the mechanism of rearrangement of solid particles starts to set in, and the significance of the latter mechanism depends on the deformation rate as well as the size of the solid particles existing in the materials. At higher deformation rate, the mechanism of rearrangement of solid particles does not have enough time to fully operate since it is a time-dependent mechanism, so other mechanisms will step in to facilitate deformation, which results in a higher deformation stress required. This phenomenon is shown by comparing Fig. 6 (lower deformation rate) with Fig. 7 (higher deformation rate) for all the materials. However, for the materials with smaller particles, the mechanism of rearrangement of solid particles is easier to operate than for those with larger particles, which results in less deformation stress required for the materials with smaller particles. This phenomenon is exhibited by comparing the S/D materials, which have smaller solid particles, with the SSS and CC materials, which have much larger solid particles. The former thus requires significantly less stress for deformation than the latter at the initial stage of the deformation, as shown in Figs 6 and 7.

For the materials with larger solid particles, such as SSS and CC materials, the mechanism of rearrangement

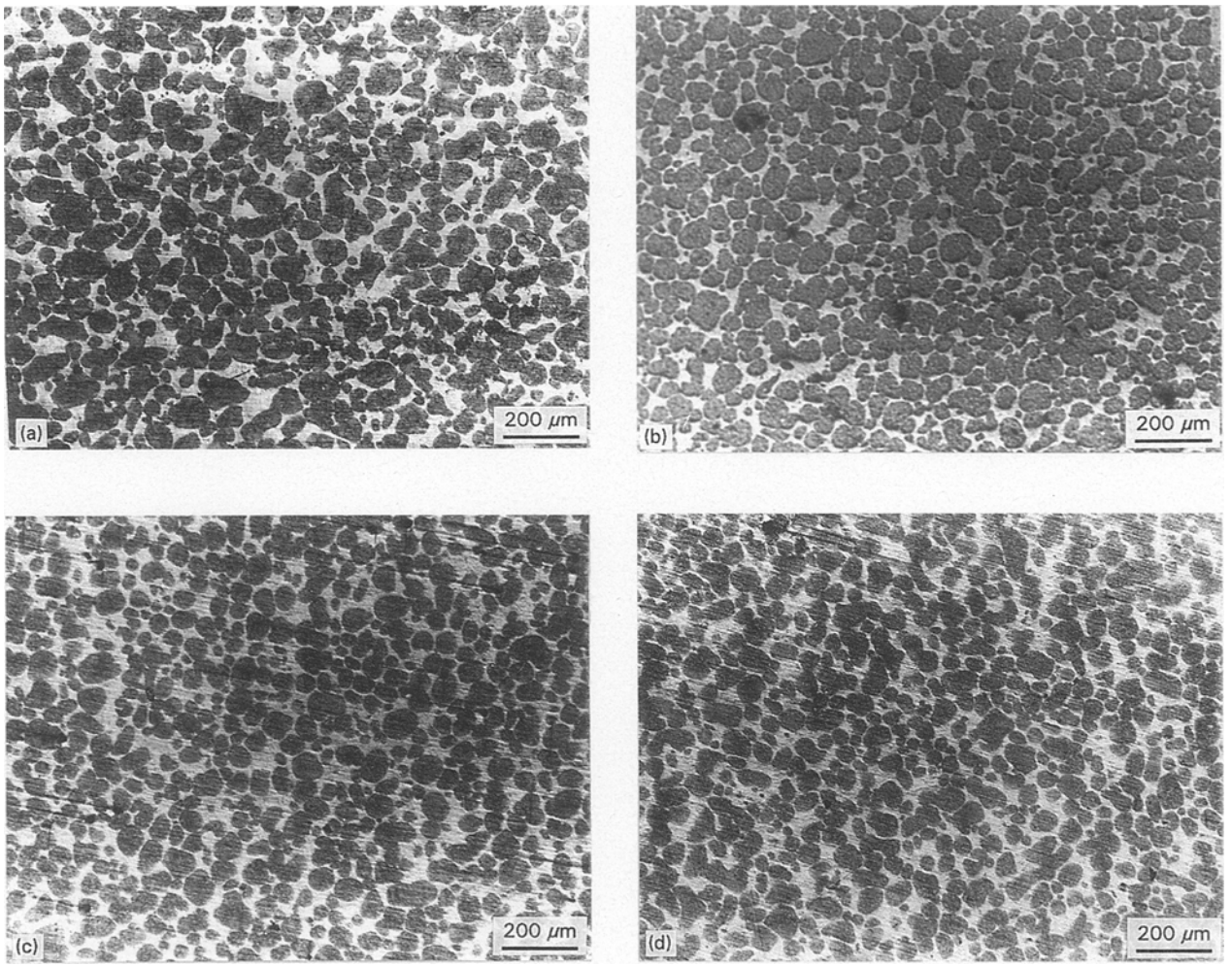

Figure 5 The microstructures of the CC material after the semi-solid deformation at (a) 190 °C, and 0.00083 s^{-1}; (b) 190 °C, and 0.083 s^{-1}; (c) 200 °C, and 0.00083 s^{-1}; and (d) 200 °C, and 0.083 s^{-1}.

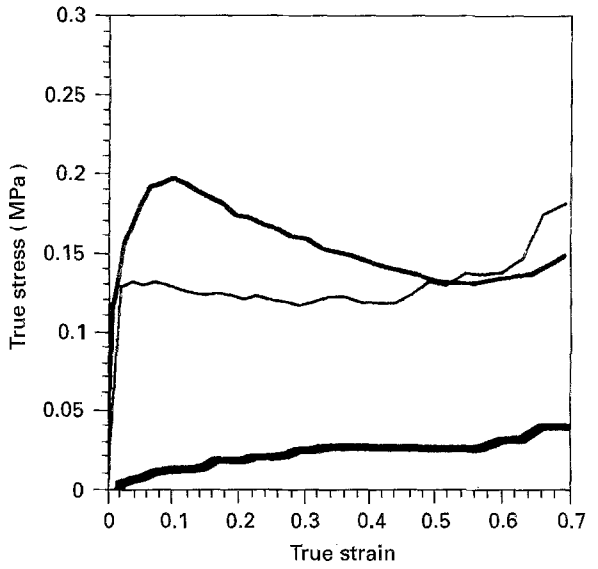

Figure 6 The stress versus strain relationships of semi-solid deforming of S/D (▬), SSS (—) and CC (—) materials at 190 °C, and 0.00083 s^{-1}.

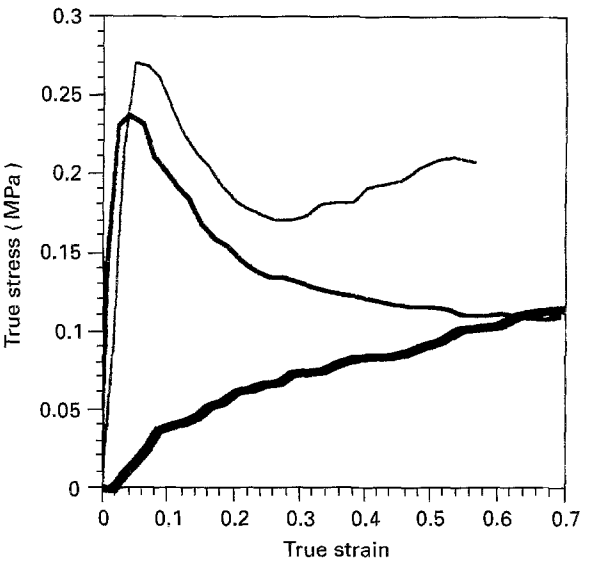

Figure 7 The stress versus strain relationships of semi-solid deforming of S/D (▬), SSS (—) and CC (—) materials at 190 °C, and 0.083 s^{-1}.

of solid particles that requires time to operate starts to be fully operative as the deformation proceeds, which results in a decrease of the deformation stress after the initial rise in stress. As the strain reaches a certain magnitude, the movement of the solid particles starts to be restricted by themselves due to an increase of the solid fraction, as most of the liquid phase has been pushed towards the edge leaving solid particles

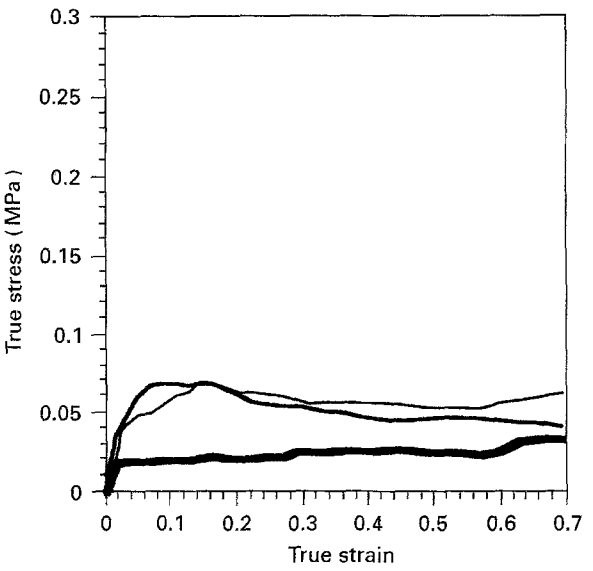

Figure 8 The stress versus strain relationships of semi-solid deforming of S/D (▬), SSS (—) and CC (—) materials at 200 °C, and 0.00083 s^{-1}.

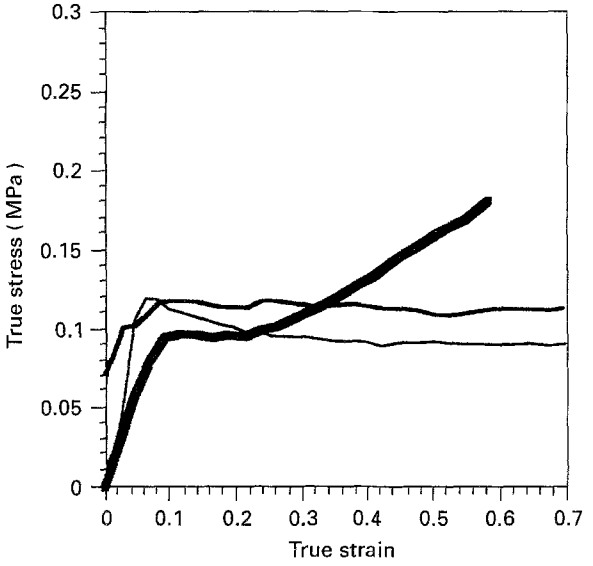

Figure 9 The stress versus strain relationships of semi-solid deforming of S/D (▬), SSS (—) and CC (—) materials at 200 °C, and 0.083 s^{-1}.

behind. At this stage, the mechanism of compression of the liquid and later the mechanism of plastic deformation of solid particles, all of which require a larger stress than the other two mechanisms, start to play a significant role. As a result, the stress starts to rise again after reaching a minimum value, as shown in Figs 6 and 7 at greater strain. As the deformation rate increases, the flowability of the liquid phase decreases, the time for particles to rearrange is less, and the ductility of the solid particles decreases, all of which result in larger deformation stress.

However, for the materials with smaller particles such as S/D materials, since the mechanism of rearrangement of solid particles is easier to be in operation from the beginning of the deformation as described previously, both of the flow of liquid and rearrangement of solid particles mechanisms operate together and incorporate with each other from the onset of the deformation. As a result, the deformation stress does not show a decrease at the initial stage of the deformation that is shown by the materials with larger particles. At larger strain, the stress continues to rise due to the operation of the mechanisms of compression of the liquid phase and plastic deformation of solid particles as indicated before.

The effects of the deformation temperature on the stress versus strain relationships of the semi-solid deformation are shown by comparing Figs 8–9 for higher deformation temperature with Figs 6–7 for lower deformation temperature. The stress–strain behaviours of all the materials for higher deformation temperatures (200 °C) show similar trends as those for lower deformation temperatures (190 °C). However, the deformation stresses for higher deformation temperature are shown to be much lower than those for lower deformation temperature due to the lower fraction of solid and better ductility of the solid particles at higher deformation temperature.

4. Conclusions

1. A physical phenomenological model is proposed to explain the different behaviours of the stress–strain curves of semi-solid forming of various materials under various conditions.
2. There is no significant variation in particle size and in sphericity during semi-solid forming of Pb-35 wt % Sn alloys at 0.083 and 0.00083 s^{-1} strain rates and at 190 and 200 °C deformation temperatures, separately.
3. The deformation stress increases monotonically as strain increases during semi-solid deformation of S/D materials, which consist of smaller solid particles.
4. For SSS and CC materials, which consist of larger solid particles, the deformation stress increases in the beginning to a local maximum, then decreases to a minimum before it starts to increase again as strain increases. This phenomenon is more notable at lower deformation temperature and higher strain rate.
5. The deformation stresses required for deformation at higher deformation rate and at lower deformation temperature are larger than those at lower deformation rate and at higher deformation temperature, respectively.

Acknowledgements

Support from the National Science Council of Taiwan under grant no. NSC 82-0405-E-006-294 is gratefully acknowledged.

References

1. M. C. FLEMINGS, *Metall. Trans. A*, **22A** (1991) 957.
2. D. H. KIRKWOOD and P. KAPRANOS, *Casting Technol.* **Jan.** (1989) 16.
3. S. B. BROWN and M. C. FLEMINGS, *Adv. Mater. Proc.* **Jan.** (1993) 36.
4. D. B. SPENCER, R. MEHRABIAN and M. C. FLEMINGS, *Metall. Trans.* **3** (1972) 1925.

5. J. F. SECONDE and M. SUERY, *J. Mater. Sci.* **19** (1984) 3995.
6. V. LAXMANN and M. C. FLEMINGS, *Metall. Trans. A* **11A** (1980) 1927.
7. M. SUERY and M. C. FLEMINGS, *Ibid.* **13A** (1982) 1809.
8. Y. S. YANG and C. -Y. A. TSAO, *Scripta Metall. et Mater.* **30** (1994) 1541.
9. C. P. CHEN and C.-Y. A. TSAO, in Advances in Powder Metallurgy, PM^2 TEC'94 Conference, MPIF-APMI, Toronto, Canada, 1994 (MPIF-APMI).
10. H. LEHUY, J. BLAIN, G. L. BATA and J. MASOUNAVE, *Metall. Trans. B* **15B** (1984) 173.
11. P. KAPRANOS, D. H. KIRKWOOD and C. M. SELLAR, *Proc. Inst. Mech. Engrs.* **207B** (1993) 1.
12. M. A. TAHA and M. SUERY, *Met. Tech.* **11** (1984) 226.
13. P. O. CHARREYRON and M. C. FLEMINGS, *Int. J. Mech. Sci.* **27** (1985) 781.
14. L. A. LALLI, *Metall. Trans. A* **16A** (1985) 1393.
15. M. KIUCHI and S. SUGIYAMA, *J. Mater. Shaping Tech.* **8** (1990) 39.
16. K. MIWA, K. KOBAYASHI and T. NISHIO, in the Third International Conference on Semi-Solid Processing of Alloys and Composites edited by M. Kiuchi (Institute of Industrial Science, Univ. of Tokyo 1994) p. 483.
17. C. A. TSAO and N. J. GRANT, in "Rapidly solidified materials: properties and processing", San Diego (ASM Int., 1988) p. 163.
18. C. -Y. A. TSAO and N. J. GRANT, *Int. J. Powder Metall.* **30** (1994) 323.
19. C. -Y. A. TSAO Ph.D. Thesis, MIT, Cambridge, MA (1990).
20. N. J. GRANT, in "Casting of near net shape products", edited by Y. Sahai, J. E. Battles, R. S. Carbonara and C. E. Mobley (The Metallurgical Society of AIME, 1988) p. 203.
21. T. ANDO, C. -Y. A. TSAO J. WAHLROOS and N. J. GRANT, *Int. J. Powder Metall.* **26** (1990) 311.
22. A. G. LEATHAM, A. J. W. OGILVY, P. F. CHESNEY and O. H. METELMANN, *Modern Developments in Powder Metallurgy* **19** (1988) 475.
23. A. G. LEATHAM, and A. LAWLEY, *Int J. Powder Metall.* **29** (1993) 321.

Received 8 November 1994
and accepted 22 March 1995